

Application of radiochromic gel dosimetry to commissioning of a megavoltage research linear accelerator for small-field animal irradiation studies

Noora Ba Sunbul^{a)}

*Department of Nuclear Engineering and Radiological Sciences, University of Michigan, Ann Arbor, MI, USA
Department of Radiation Oncology, University of Michigan, Ann Arbor, MI, USA*

Ibrahim Oraiqat

*Department of Radiation Oncology, University of Michigan, Ann Arbor, MI, USA
H. Lee Moffitt Cancer Center and Research Institute, Tampa, FL 33612, USA*

Benjamin Rosen

Department of Radiation Oncology, University of Michigan, Ann Arbor, MI, USA

Cameron Miller and Christopher Meert

Department of Nuclear Engineering and Radiological Sciences, University of Michigan, Ann Arbor, MI, USA

Martha M. Matuszak

*Department of Nuclear Engineering and Radiological Sciences, University of Michigan, Ann Arbor, MI, USA
Department of Radiation Oncology, University of Michigan, Ann Arbor, MI, USA*

Shaun Clarke and Sara Pozzi

Department of Nuclear Engineering and Radiological Sciences, University of Michigan, Ann Arbor, MI, USA

Jean M. Moran

Department of Radiation Oncology, University of Michigan, Ann Arbor, MI, USA

Issam El Naqa

*Department of Radiation Oncology, University of Michigan, Ann Arbor, MI, USA
H. Lee Moffitt Cancer Center and Research Institute, Tampa, FL 33612, USA*

(Received 1 May 2020; revised 25 November 2020; accepted for publication 17 December 2020; published 6 February 2021)

Purpose: To develop and implement an efficient and accurate commissioning procedure for small-field static beam animal irradiation studies on an MV research linear accelerator (Linatron-M9) using radiochromic gel dosimetry.

Materials: The research linear accelerator (Linatron-M9) is a 9 MV linac with a static fixed collimator opening of 5.08 cm diameter. Lead collimators were manually placed to create smaller fields of $2 \times 2 \text{ cm}^2$, $1 \times 1 \text{ cm}^2$, and $0.5 \times 0.5 \text{ cm}^2$. Relative dosimetry measurements were performed, including profiles, percent depth dose (PDD) curves, beam divergence, and relative output factors using various dosimetry tools, including a small volume ionization chamber (A14), GAFCHROMIC™ EBT3 film, and Clearview gel dosimeters. The gel dosimeter was used to provide a 3D volumetric reference of the irradiated fields. The Linatron profiles and relative output factors were extracted at a reference depth of 2 cm with the output factor measured relative to the $2 \times 2 \text{ cm}^2$ reference field. Absolute dosimetry was performed using A14 ionization chamber measurements, which were verified using a national standards laboratory remote dosimetry service.

Results: Absolute dosimetry measurements were confirmed within 1.4% ($k = 2$, 95% confidence = 5%). The relative output factor of the small fields measured with films and gels agreed with a maximum relative percent error difference between the two methods of 1.1 % for the $1 \times 1 \text{ cm}^2$ field and 4.3 % for the $0.5 \times 0.5 \text{ cm}^2$ field. These relative errors were primarily due to the variability in the collimator positioning. The measured beam profiles demonstrated excellent agreement for beam size (measured as FWHM), within approximately 0.8 mm (or less). Film measurements were more accurate in the penumbra region due to the film's finer resolution compared with the gel dosimeter. Following the van Dyk criteria, the PDD values of the film and gel measurements agree within 11% in the buildup region starting from 0.5 cm depth and within 2.6 % beyond maximum dose and into the fall-off region for depths up to 5 cm. The 2D beam profile isodose lines agree within 0.5 mm in all regions for the $0.5 \times 0.5 \text{ cm}^2$ and the $1 \times 1 \text{ cm}^2$ fields and within 1 mm for the larger field of $2 \times 2 \text{ cm}^2$. The 2D PDD curves agree within approximately 2% of the maximum in the typical therapy region (1–4 cm) for the $1 \times 1 \text{ cm}^2$ and $2 \times 2 \text{ cm}^2$ and within 5% for the $0.5 \times 0.5 \text{ cm}^2$ field.

Conclusion: This work provides a commissioning process to measure the beam characteristics of a fixed beam MV accelerator with detailed dosimetric evaluation for its implementation in megavoltage small animal irradiation studies. Radiochromic gel dosimeters are efficient small-field relative dosimetry tools providing 3D dose measurements allowing for full representation of dose, dosimeter misalignment corrections and high reproducibility with low inter-dosimeter variability. Overall, radiochromic gels are valuable for fast, full relative dosimetry commissioning in comparison to films for application in high-energy small-field animal irradiation studies. © 2020 American Association of Physicists in Medicine [https://doi.org/10.1002/mp.14685]

Key words: animal irradiator and small-field dosimetry, commissioning, gel dosimetry

1. INTRODUCTION

The planning and delivery of radiotherapy have been steadily becoming more complicated with sophisticated tools for daily image-guidance. These advances have rendered simple X-ray irradiators based on kilovoltage and orthovoltage X-ray machines incompatible with modern linear accelerator treatment delivery complexity. Hence, there is a burgeoning interest in developing small animal irradiators to scale down this complex system for radiobiological research.¹ These research irradiator devices use ionizing radiation as either X-rays or gamma rays for animal irradiation studies. Kilovoltage irradiators operate in the beam energy range of 10–120 kV, while orthovoltage units operate from 130 to 320 kV. These low-energy irradiators can be used for either whole body, partial body or organ specific irradiations with a penetration depth from 0 to 2 cm.² Due to the limited energy range of animal irradiators, applications are restricted to small animals and superficial irradiations. However, high-energy electron and photon irradiations for animal studies are possible with linear accelerators designed for clinical studies, i.e., the multi-modalities animal RT system (MultiART). MultiART is constructed by adopting existing commercial modalities such as Varian Clinac linac or SkyScan micro-CT to produce three different modes including kV and MV photon modes and MeV electron mode.³ Image guided animal irradiators have been developed for higher accuracy in replicating clinical image guided radiation therapy with dose characteristics similar to the kV and orthovoltage irradiators.⁴

Two common animal irradiator systems have been made commercially available: the Small Animal Radiotherapy Research Platform (SARRP) from Xstrahl Life Sciences developed at Johns Hopkins University, and the X-Rad SmART from Precision X-ray Inc developed at Princess Margaret Hospital.^{5–8} While these commercially available image guided irradiators are in the kilovoltage range, the megavoltage irradiators are generally custom-developed from clinical linear accelerators. In this work, we discuss the commissioning process for repurposing a 9 MV research linear accelerator as a small animal irradiator, capturing the megavoltage range of interest for relevant research purposes. While kilovoltage irradiators can mimic the clinical geometric setting, they lack effectiveness when considering preclinical radiobiological studies. Hence, the Linatron with its MV energy capabilities is more applicable for dosimetric and radiobiological

studies mimicking the clinical dose responses especially for deep dose measurements with the MV energy beam.

Machine commissioning and quality assurance (QA) measurements of linear accelerators (linacs) are key components for accurate radiation therapy treatments. With advanced treatment planning and delivery techniques, comprehensive QA and commissioning are typically performed with a range of dosimeters to sample 3D volumes. Commonly used dosimetry tools such as ionization chambers, diodes, and Gafchromic films, could provide either point measurement or 2D dose distributions. With the increasing use of complex treatment plans and delivery techniques, more precise treatment planning verification dosimetry tools are needed. Gel dosimeters have gained recent interest in research due to their ability to precisely measure dose in 3D with relatively high resolution (sub mm spatial resolution).⁹

Several recommendations and guidelines were published to develop quality assurance procedures and to verify the dose delivery of clinical linear accelerators.^{10–12} It is strongly recommended that protocols and guidelines similar to those used in commissioning animal irradiators and preclinical radiation research platforms be developed to maximize their impact in translating radiotherapy-related research into the clinic.^{13,14} The aim of the comprehensive commissioning process is to fully characterize the dosimetric characteristics of the accelerators to reach a level of accuracy that is close to that employed for clinical radiation therapy irradiation (to deliver point dose values within 5% error¹⁵).

As a result, there are various publications describing the commissioning and dosimetric beam characterization of commercially available small animal irradiator systems.^{16–23} Because commercially available animal irradiators are kV X-ray beam-based accelerators, the commissioning process is recommended to follow the American Association of Physicists in Medicine Task Group #61 (TG61) report.¹⁴ The Commissioning procedure of those commercial systems consists of output measurements and absolute dosimetry. The output factors have been measured in the literature using a suitable ionization chamber, radiochromic films, EDGE detector (diode) and gels.^{16,17,19,24} However, a previous study¹⁷ has shown that conventional dosimeters like ion chambers and diodes are not practically accurate due to volume averaging effects in small fields and demonstrated close agreement between EBT2 film and PRESAGE dosimetry for relative dosimetry measurements for fields larger than 10 mm in size.

On the other hand, absolute dosimetry measurements have been performed in the literature using calibrated ionization chambers,^{16,17,19} and alanine.²⁵

One of the main challenges in the commissioning process is the lack of independent dose verification process to assess the accuracy of dose delivery of the animal research irradiators. It has been recommended to follow a well-designed dose verification procedure for absolute dose verification to decrease uncertainties and to monitor dose delivery.²⁵

With the increase in treatment planning and dose delivery complexity, there is an increased need for quality assurance for the treatment unit and patient-specific dose delivery validation. 3D gel dosimetry is a promising dosimetry tool to verify advanced treatment delivery such as Intensity Modulated (IMRT), and Volumetric Arc Radiation Therapy (VMAT). One of the main applications of gel dosimeters is in basic dosimetry measurements because it has the capability to measure the dose distribution throughout a three-dimensional volume. Hence, it has advantages over many conventional dosimeters applied in basic electron and photon dosimetry parameter measurements such as beam profiles and percent depth doses.^{26–29}

In order for a 3D dosimetry tool to be clinically useful, the Resolution-Time-Accuracy-Precision (RTAP) performance criteria proposed by Mark Oldham *et al.* should be fulfilled. An ideal 3D dosimetry system, including the dosimeter and associated readout, is defined under RTAP to be able to deliver 3D dose measurements with 1 mm isotropic spatial resolution in less than one hour with an accuracy of 3% and a precision of 1%.³⁰

Gels are chemical dosimetry systems that are imaged with readout systems to quantify their response to radiation. There are several 3D dosimeters such as normoxic polymer gels, radiochromic plastics (i.e., PRESAGE) and radiochromic gel dosimeters. The main imaging modalities used for 3D dose readout are MRI,³¹ optical CT (optCT) and X-ray computed tomography (CT).^{9,13,32–34} Optical CTs are analogous to the common X-ray CT in their scanning principle except that they use a visible light source. The motivation for developing the X-ray (CT) and optCT readout systems was the desire to make 3D imaging readout more readily available and easily accessible.^{9,35–37}

The dose quantifications for 3D dosimetry systems using MRI results is based on the dependence between the dose and the nuclear magnetic relaxation (NMR) properties of the dosimeter under irradiation.^{9,13,38} While the dose quantification in optCT-based dosimeters is based on the radiation-induced changes in the transparency of the color of the dosimeter material at visual wavelengths which enables optCT imaging and hence dose quantification.³⁹ For radiochromic dosimeters, the optical response is a primary result of absorption based light attenuation, which has the advantage of minimal scattered light perturbation.

Previous studies have shown that certain polymer gel dosimeters are dose rate dependent, which could result from competing radiation-induced chemical reactions. This effect has been more pronounced in normoxic THP-based methacrylic

acid (MAc) gel dosimeters than in poly-acrylamide-gel (PAG) dosimeters.^{40–43} The commonly used radiochromic polymer gel PRESAGE™ is designed for use with optical CT. It has the advantages of high resolution, relatively low noise, and linear optical response to radiation dose to within 1%. However, it has little dependency on dose rate (~2%).^{29,44}

Clearview gels (Modus Medical, London, Ontario) are radiochromic 3D dosimeters designed by Modus Medical Devices Inc to be read by Optical-CT (Modus Medical, London, Ontario).⁴⁵ After gels have been exposed to ionizing radiation, their clear color changes to pink/purple due to the formation of a formazan dye within the gel.⁴⁶ The measurement dose range is 10–80 Gy, and gels have been shown to have a linear dose response up to 80 Gy, and to be independent of photon beam energy (4–18 MV) and dose rate (up to 9.9 Gy/min).⁴⁶ The post-irradiation dose stability has been studied and shown to be consistent for at least one week post-irradiation with uniform inter-batch stability.⁴⁷ Based on these characteristics, gels provide benefits for relative dosimetry; however, gels have been shown to have a limited detectability of the surface and near surface doses up to 4–5 mm depths due to the reconstruction artifacts.^{17,47}

Small radiation fields are defined as those fields that may lack charged particle equilibrium due to their smaller field size relative to the lateral range of the charged particles.¹² Because the commonly used dosimeters are considered large with respect to the small fields, this study aims to verify the 3D relative dosimetry applicability of Clearview gel dosimeters for small radiation field measurements. The verification is performed through the detailed characterization and commissioning of a 9 MV research Linatron as a small-field animal irradiator intended to capture MV physical and biological interactions. Radiochromic Clearview gels have the advantage of independent dose rate response over the more commonly used polymer gels. In this work, the feasibility of Clearview gels as a relative 3D dosimetry tool is tested for accuracy and efficiency by capturing the percent depth dose curves, beam profiles and relative output factors (ROFs) of different small fields in comparison to EBT3 Gafchromic films.⁴⁸

2. MATERIALS AND METHODS

2.A. The research small-field linear accelerator

The research linear accelerator (Linatron-M9) is a 9 MV flattening-filter-free photon-mode accelerator that has a fixed target and a single electron energy mode (9 MeV), which produces a “9 MV” bremsstrahlung photon beam.⁴⁹ The Linatron has a static beam with a horizontal collimator opening of 5.08 cm in diameter to shape a static circular beam size, FWHM, of approximately 7.5 cm in diameter at the calibration point of 220 cm from the source target. This Linatron was originally installed for active interrogation nuclear material detection research. Hence, for the repurposing of the Linatron as a small animal irradiator, lead collimation bricks were manually placed at the exit of the beam as a secondary collimator to shape the beam to smaller fields of $2 \times 2 \text{ cm}^2$,

$1 \times 1 \text{ cm}^2$ and $0.5 \times 0.5 \text{ cm}^2$ horizontal beams (Fig. 1) at the calibration point of 220 cm source to surface distance (SSD). This manual collimation of the beam allows for a simple repurposing of the Linatron to widen its research applicability as an MV small-field animal irradiator. Positioning lasers were manually integrated to the Linatron to increase collimator and phantom positioning reproducibility and reduce alignment errors [Fig. 1(a) and 1(b)].

As previously mentioned, the effective point of calibration and measurement SSD was located at 220 cm. Measurement points were selected to balance the SSD (for machine output) and adequate distance for the measurement setup. The Linatron output (LO) is controlled either in the unit of irradiation time (seconds) or as the total dose (Gy) by the built-in ionization chamber monitor placed at 100 cm from the source.

2.B. Absolute dosimetry measurement

Absolute measurement of the Linatron output was performed using a 15 mm^3 effective volume thimble ionization chamber (A14).⁵⁰ The output measurements were performed for the machine-specific static collimated field of the Linatron, 7.5 cm in diameter beam size at 220 cm SSD. All correction coefficients including recombination, polarity, pressure, and temperature were applied following the AAPM TG-51 calibration protocol.¹¹ However, due to the geometrical constraints of this system, it is impractical to reach the reference condition of 100 cm SSD, as reported in the TG51 recommendations. Some modifications had been made to the AAPM TG51 protocol, due to the difference in dimensions and accessibility of the Linatron machine compared to a clinical machine. The ionization chamber was cross-calibrated using a clinical Varian TrueBeam linac (Varian Medical Systems, Palo Alto, CA) to ensure higher accuracy of our dose calibration method. The beam quality of the Linatron was simulated using EGSnrc (BEAMnrc/DOSXYZnrc) Monte Carlo codes in a water phantom and verified in a solid water measurement using the tissue phantom ratio (TPR) at depths

of 20 and 10 cm (TPR20/10) for a field of 11.28 cm diameter (10 cm x 10 cm square equivalent field).^{10,51,52} The relative percentage error between the two methods was $\sim 0.16\%$.

The absolute Linatron output stability was measured during its daily operations (at different operation hours) on two different weeks within a month-long period. The variation of the daily first Linatron operation output was measured for each weekly experimental operation of the Linatron during that measurement month. The time linearity of the Linatron output (in minutes) was measured and verified with the A14 ionization chamber dose measurement in Gy [Fig. 1(a)].

2.C. Clearview gel measurement

3D dosimetry measurements including PDD curves, beam profiles and output factors of the small fields were performed using different Clearview gel dosimeter jars (Modus Medical Devices Inc.).⁴⁵ The gel jars were from two different batches; therefore, each batch was calibrated separately. Each field was measured three times using the same dosimeter jar while allowing enough separation between the fields in order to not affect the measured dose distributions.^{17,53} All experiments were acquired at the same SSD, 220 cm from the Linatron target, at a relative inter-gel depth of 2 cm [Fig. 1(b)]. SSD and depth of measurements were selected because the reference conditions specified in the standard dosimetry protocols¹¹ for beam calibrations cannot be met for this accelerator.

Dose profiles were extracted at a depth of 2 cm for all fields. Gel dosimeters were scanned with a Vista optical CT scanner Model: 16 (Modus Medical, London, ON). The resolution was set to 0.5 mm for all scanned gels using the iterative back projection image reconstruction technique for better scanning and image resolution than the simple back projection reconstruction.⁵⁴ The jars were marked for accurate repositioning of the dosimeter in reference to the background correction scan. All the gels were scanned pre-irradiation exposure to compensate and correct for the background

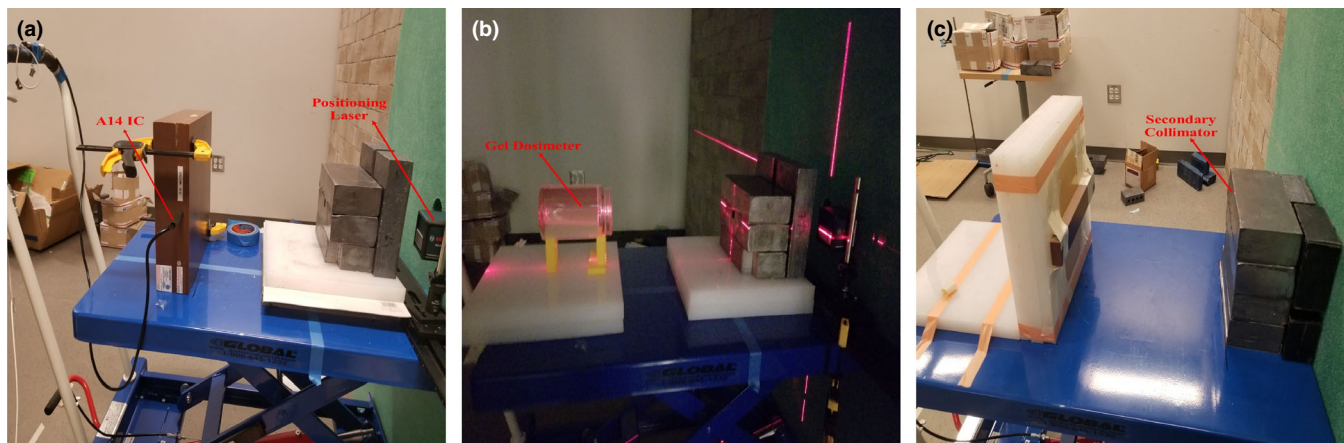


FIG. 1. Relative and absolute dosimetry measurement setup at 220 cm SSD and effective measurement depth of 2 cm in phantom (2 cm buildup thickness of solid water (a,c) or gel (b)) (a) measurements setup using A14 ionization chamber (b) radiochromic gel jar (c) film measurement. (b) shows the integrated positioning lasers used to increase collimator and phantom positioning reproducibility and reduce production errors. [Color figure can be viewed at wileyonlinelibrary.com]

reading following manufacturer recommendations. All jars including the calibration and measurements were scanned within 24 hr of exposure to ensure signal stability. Each batch of gels was calibrated using a 9 MeV electron beam to provide absolute dosimetry readings.

The gel calibration was performed using a clinical Varian TrueBeam linac (Varian Medical Systems, Palo Alto, CA) to ensure higher accuracy of the dose calibration. A 9 MeV electron beam using the standard 10 cm × 10 cm cutout, with SSD = 100 cm, and 30 Gy delivered to dmax (2.0 cm) was used. The gel central-axis attenuation coefficient change (i.e., optical density change) was measured using the Vista Optical-CT and fitted linearly with the corresponding central-axis depth dose. The 9 MeV electron beam calibration is recommended by the gel manufacturer so that a full depth dose curve (100% to <5%) can be measured using a single gel phantom. The electron beam is a simple way of compressing a wide dynamic dose range into the space of the jar.⁵⁵ The calibration curves were then obtained using a linear fit to relate the optical density to dose in Gy as shown in Fig. 2(a). This calibration procedure is sufficient only for relative dose measurements and is insufficient for absolute dosimetry due to potential energy dependence concerns. Gel analysis was performed using in-house developed MATLAB codes that have been validated using spot checks and redundancy algorithms. The common procedure that was adopted for the gel measurement is:⁴⁷

1. gels were stored at ~4°C temperature (in a refrigerator)
2. gels were returned to room temperature prior to irradiation (approximately 8 hr before irradiation gels were removed from refrigerator)
3. gels were read at room temperature,
4. gels were sheltered from light as much as possible during transport, setup, and handling using light-tight opaque bags.

2.D. Film measurement

EBT3 Gafchromic films (Ashland, Bridgewater, NJ)⁴⁸ were used in the same measurement setup as the gels for 2D

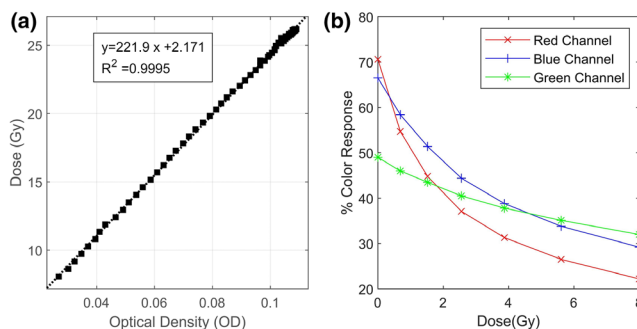


FIG. 2. (a) Clearview gel calibration curve relating optical density to dose in Gy and (b) the three color (red, blue, green) components of the film calibration curve relating the percent color response of the film to dose in Gy. [Color figure can be viewed at wileyonlinelibrary.com]

relative dosimetry measurements of PDDs, ROFs, beam profiles and beam divergence. Solid water (Gammex Solid water) slabs of 2 cm thickness were used for dose buildup [Fig. 1(c)].

Films were scanned with EPSON scanner Model: EU-88 set to the professional mode. The resolution was set to 150 dpi for all scanned films. All calibration and measurement films were scanned at least 24 hr after the film exposure to ensure adequate film saturation before scanning.⁵⁶ The scanned films were analyzed using FilmQA Pro (Ashland Scientific software⁵⁷) and MATLAB codes following the AAPM (TG-47) specifications.⁵⁸ All the films were exposed for at least 2 min to decrease the effect of noise and, therefore, the associated errors that are expected at the small optical density values.⁵⁶

The film calibration curve was established for doses ranging from 0 (un-irradiated film) up to 8 Gy [Fig. 2(b)]. The unirradiated film was used to determine the necessary background correction, while the 8 Gy film represents the maximum expected measured dose. The radiochromic films were calibrated using the three color components: red, green and blue. However, the analysis was performed using the red color component since it has higher sensitivity.⁵⁹

All measurements were reported as the average of three different trials to inherently assess the overall reproducibility of the measurement using gels and films. The accuracy of the secondary collimator setup (the manual collimator positioning misalignment) was measured by evaluating the variability among six different trials (three different setups per person). The collimator positioning uncertainty is estimated as the standard deviation of the measured output (D_{max}) of the field, with D_{max} referring to the maximum dose at the central $2 \times 2 \text{ mm}^2$ ROI of both the $0.5 \times 0.5 \text{ cm}^2$ and the $2 \times 2 \text{ cm}^2$ fields.

2.E. Commissioning applicability in animal irradiations

After the full commissioning, the Linatron was applicable as an animal irradiator for rabbit irradiation and dose measurements (Fig. 3). The Linatron output measured with A14 IC in Gy was calculated to estimate and control the intended dose at the point of irradiation for animal irradiation studies. The relative output factor of the $2 \times 2 \text{ cm}^2$ field of interest in the animal irradiation work was measured relative to the open Linatron field with A14 IC and verified with the film measurements. Hence, the measurement dose at the point of irradiation for all fields can be calculated using the MU formula recommended by TG-71.⁶⁰ The absolute dosimetry accuracy was verified in-house with an A14 ionization chamber and then independently with a TLD using a remote dosimetry service. The remote dosimetry service included TLD calibration, analysis and readouts and was performed at the University of Wisconsin-Madison Radiation Calibration Laboratory for more accurate measurement of the output reproducibility and calibration effectiveness.

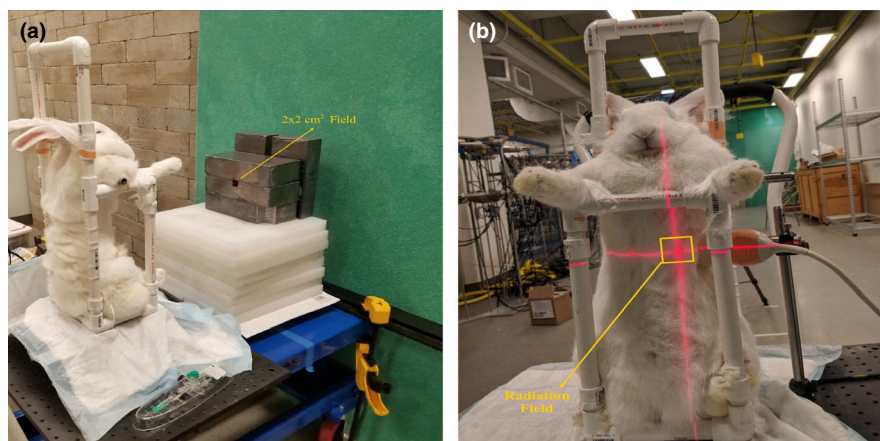


FIG. 3. Example rabbit irradiation setup showing the utilization of commissioned Linatron in small animal irradiation studies. (a) A euthanized rabbit was supported vertically with built-in holder and exposed to a 2×2 cm² field at 220 cm SSD (b). The total maximum dose was maintained to be <20 Gy per fraction as per the institutional animal protocol.⁶¹ [Color figure can be viewed at wileyonlinelibrary.com]

3. RESULTS

3.A. Linatron output constancy and time linearity

The Linatron output is controlled either per time unit or as total dose (cGy). IC measurements were performed to verify the Linatron output (cGy/min) variability with time and by measuring the timer-to-output Linatron linearity. The Linatron output variability with time after the first irradiation was measured on two different days within a month period with a standard deviation between the absolute dose readings of 0.61% and 0.48% on the first and second day. The Linatron output increases with time after its first operation. The variability of the Linatron output at its first operation was 0.51% corresponding to absolute dose variability measured with A14 IC weekly of 0.55% on four different days over nearly a month. Overall, the reported variability of the Linatron during its expected operational hours is <1% (Tables I and II) as verified with the measured dose of A14 IC. The total dose measured at variable irradiation times (minutes) was found to follow a linear trend as expected with a reported R^2 value of 1 based on the A14 IC dose readings in cGy and the Linatron output reading as well (Fig. 4). The Linatron output rate (cGy/min) remained relatively constant during the total irradiation time with an average of 600.44 ± 0.76 cGy/min which was verified with the A14 IC to be 145.60 ± 0.29 cGy/min.

3.B. Small-field relative dosimetry

The full 3D dose distributions were measured with gels (Fig. 5) and used to extract beam characteristics and relative dosimetry including beam profiles, PDDs and ROFs. The relative dose gel results were then compared with the 2D dose distributions extracted at the corresponding orientation using films.

3.C. Beam profiles

The average beam profiles, expressed as full width at half maximum (FWHM), were measured with gels and films (Fig. 6 for horizontal and vertical beam profiles). The main characteristics of each small field, such as FWHM and (20–80%) penumbras, are listed in Table III. The overall average collimation positioning uncertainty was measured to be 1.93% and 4.18% for the 2×2 cm² and the 0.5×0.5 cm² field, respectively.

3.D. Percent dose depth curves

Figure 7 shows the measured percent depth dose (PDD) curves for the three small fields. Data were measured with both EBT3 Gafchromic films and gel dosimeters. Each curve is represented as the average of three different measurement trials. The error bars are reported as the standard deviation

TABLE I. Daily Linatron output variability with time (intra-day variability) for 3 min of irradiation.

Irradiation time (Hours)	5/3/2019		5/4/2019	
	Absolute Dose (cGy/min)	Linatron Output Reading (cGy/min)	Absolute Dose (cGy/min)	Linatron Output Reading (cGy/min)
0.00	146.41 ± 0.49	601.23 ± 0.81	146.64 ± 0.85	603.5 ± 0.95
2.50	147.97 ± 0.28	600.67 ± 1.28	148.05 ± 0.38	601.47 ± 0.36
3.50	148.52 ± 0.47	601.40 ± 0.69	--	--

TABLE II. First operation Linatron output variability with date of exposure (inter-day variability).

Date of irradiation	Absolute Dose (cGy/min)	Linatron Output Reading (cGy/min)
5/3/2019	146.41 ± 0.49	601.22 ± 0.81
21/3/2019	144.58 ± 0.32	595.42 ± 0.86
5/4/2019	146.64 ± 0.85	603.5 ± 0.95
11/4/2019	145.57 ± 0.11	597.76 ± 11.84

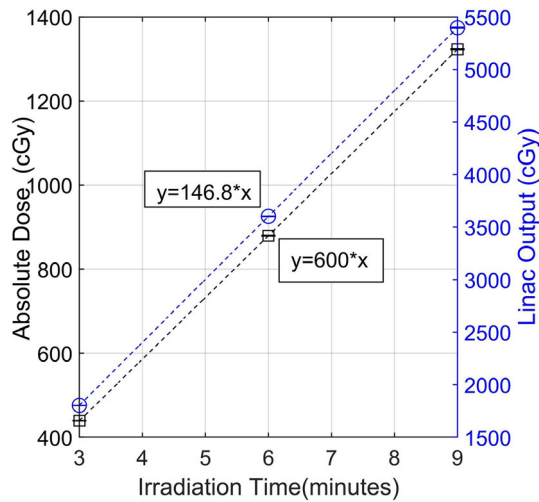


FIG. 4. Linatron output-timer linearity absolute measurement verification with A14 IC; absolute total dose measured as the average of three different trials and the error is the standard deviation between trials. The smaller error bars (much smaller than the marker sizes) represent the uncertainty in the measurements. [Color figure can be viewed at wileyonlinelibrary.com]

between the individual readings. Both film and gel curves were normalized to the average maximum measured dose. The PDD values from the film and gel measurements agree within 11% in the buildup region starting from 0.5 cm depth and within 2.6 % at tail region depths up to 5 cm.

3.E. Relative output factors

The output factors for the small fields were measured relative to the 2 × 2 cm² collimated field and are reported in Table IV. Film and gel output factor measurements were calculated at the reference depth of 2 cm in a region of interest of 2 × 2 mm² for the three field sizes measured. The reference depth of 2 cm was selected to simplify the Linatron output dose calculations for animal irradiations as it is the estimated skin to liver distance for rabbit measurement applications. The relative percent difference between gel and film measurements was 1.1 % for the 1 × 1 cm² field and 4.3 % for the 0.5 × 0.5 cm² field. The major contribution to this error was the manual positioning of the collimator, as both measurements were performed on different days and with independent manual collimation setups.

The output factor for the 2 × 2 cm² field and the 0.5 × 0.5 cm² was reported as three different trials per person to decrease the effect of the collimation positioning in the overall measurement and ensure compatibility with the gel results, which were performed at a different collimation setting.

3.F. Beam divergence and inverse-square law

Measurements were performed for the open 5.08 cm diameter field size using EBT3 Gafchromic films at different SSDs to measure the divergence of the beam (Fig. 8). The beam field size diverges linearly with SSD. The measured beam size, FWHM, values agree with the mathematically expected beam divergence values within ~1.8% difference except at the beam exit point due to the collimation positioning uncertainty in beam exit collimation (Table V).

Fitting the absolute dose values measured with film to the SSD distances results in an inverse square fitting with an R² of nearly unity (0.999), as expected due to the inverse-square law (Fig. 9). Variations in solid water positioning used for 2-cm buildup led to some profile asymmetry, which affected

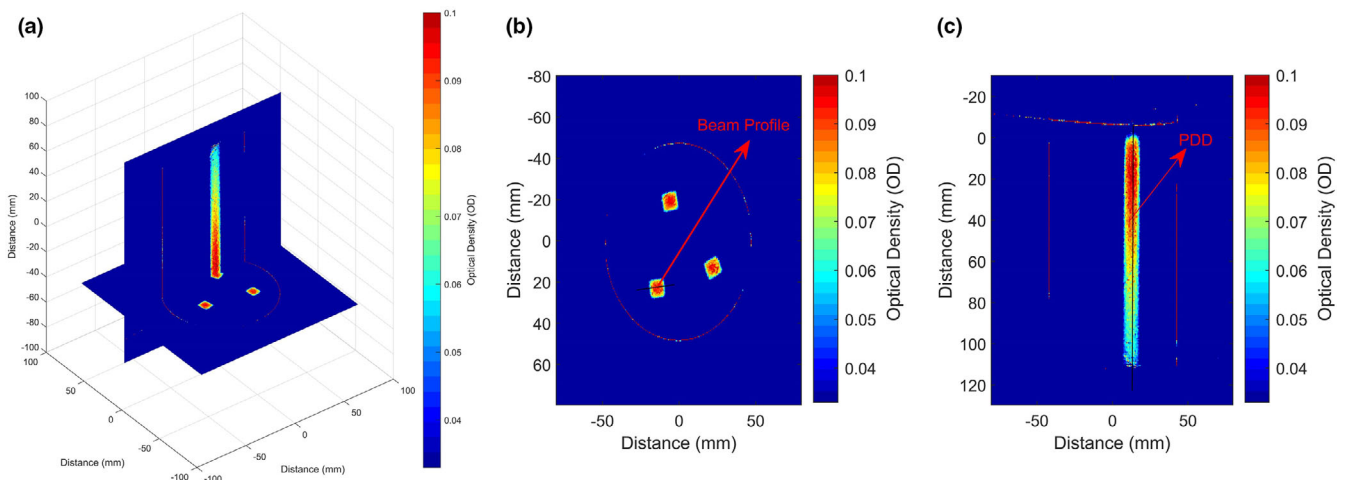


FIG. 5. 3D view of gel dose measurements (in optical density OD) per pixel position for the 1 × 1 cm² field showing the transverse and sagittal views of dose distributions in b, c for extracting beam profiles at 2 cm depth, and PDD curves respectively. [Color figure can be viewed at wileyonlinelibrary.com]

the scatter for film divergence measurements and hence beam symmetry (Fig. 8).

3.G. 2D contour plots of clearview gel compared with film

3.G.1. Beam profile

The profile contour plots were extracted at a depth of 2 cm for all field sizes using both the EBT3 and Clearview gels, as shown in Fig. 10. The isodose lines agree within 0.5 mm for all fields up to $1 \times 1 \text{ cm}^2$ and within 1 mm for the $2 \times 2 \text{ cm}^2$ field. Overall, these isodose lines show excellent agreement for the three fields, taking into consideration the small dimension of the fields and the differences in the resolution of the imaging modalities used in this study.

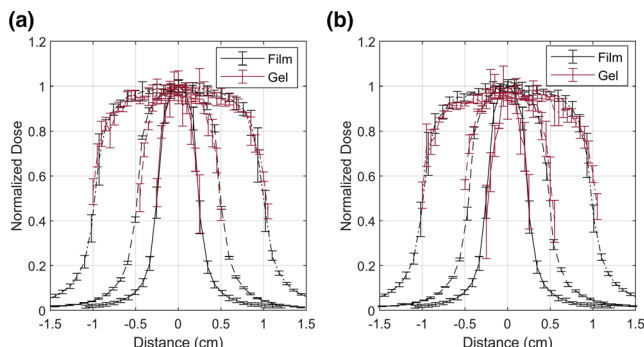


FIG. 6. Beam profiles of the $0.5 \times 0.5 \text{ cm}^2$, $1 \times 1 \text{ cm}^2$ and $2 \times 2 \text{ cm}^2$ fields measured with gel dosimeter and EBT3 films at 2 cm reference depth in phantom; (a) the horizontal (in plane) beam profiles, (b) is the vertical (cross plane) beam profiles. Due to limited sensitivity of the gels for low doses, gel profiles were limited to absolute doses above 8 Gy. [Color figure can be viewed at wileyonlinelibrary.com]

3.G.2. PDD curves

Figure 11 compares the curves acquired from the film and the Clearview gels at the central beam region along the beam direction. All curves agree within approximately 2% of the maximum in the typical therapy region (1–4 cm). The EBT3 curves were slightly steeper (~12% at 2.5–4 cm) for the $0.5 \times 0.5 \text{ cm}^2$ field. The main contribution of this

difference is film misalignment, which causes the curve to fall off more steeply for films in comparison to gel. As measured in this study, there is an inherent approximated collimation placement error of 4.18% for the $0.5 \times 0.5 \text{ cm}^2$ field, which also contributes to the discrepancy as both measurements were performed at different collimation setup. A correction factor relating the PDD measurement along the beam direction at 2 cm to the output dose measured across the beam direction at 2 cm depth was applied to correct for the film positioning relative to the beam center. This approach improved the agreement between the film and gel measured PDD curves to be within approximately 5% in the typical therapy region (1–4 cm) as shown in Fig. 11(a).

Overall, film measured PDDs are steeper than those of the gel for all the fields. The main cause of this effect is not clearly known and as stated in literature the main causes are the expected reduction in the accuracy of film data at depths deeper than 2 cm. Additionally, the film misalignment would cause the curve to decrease more steeply. The relative differences in electron density of the EBT3 film and gels could contribute to this effect as well.

3.H. Commissioning applicability in animal irradiations

The Linatron calibration factor was measured to be $600.93 \pm 1.12 \text{ cGy/min}$. While the output factor of the $2 \times 2 \text{ cm}^2$ relative to the reference circular field of 5.08 cm diameter was measured with both A14 IC and verified with films to equal 0.94 ± 0.002 and 0.94 ± 0.02 , respectively. The absolute dosimetry accuracy was verified by exposing two separate dosimeters (A14 IC and TLD) to a total dose of 100 cGy. The average readings of both were 101.37 ± 0.52 , $101.09 \pm 0.57 \text{ cGy}$, respectively. The Linatron output is hence measured and verified with an error of <1.4%.

4. DISCUSSION

The dose linearity with exposure time of the Linatron was tested for only the expected operational duration of the Linatron for animal studies (up to approximately 10 min). The overall output variability is always less than 1% after a few hours of noncontinuous operation (Tables I and II). The lead collimator positioning uncertainty contributes to the higher uncertainty in the measurement reproducibility especially for

TABLE III. Beam profile characteristics at 2 cm depth in phantom using films and gels.

	Field Width (cm)		Left Penumbra (cm)		Right Penumbra (cm)	
	Film	Gel	Film	Gel	Film	Gel
$0.5 \times 0.5 \text{ cm}^2$	0.48 ± 0.04	0.50 ± 0.01	0.15 ± 0.02	0.19 ± 0.11	0.15 ± 0.01	0.20 ± 0.09
$1 \times 1 \text{ cm}^2$	0.96 ± 0.03	0.99 ± 0.05	0.20 ± 0.02	0.23 ± 0.07	0.20 ± 0.07	0.22 ± 0.01^a
$2 \times 2 \text{ cm}^2$	1.98 ± 0.01^a	2.06 ± 0.01^a	0.26 ± 0.01	0.35 ± 0.02	0.34 ± 0.01^a	0.24 ± 0.01

^aA minimum error value in measurement of 0.01 cm is reported here for the beam profiles extracted from film. Similarly, for the error value in the right penumbra measured with both gel and films.

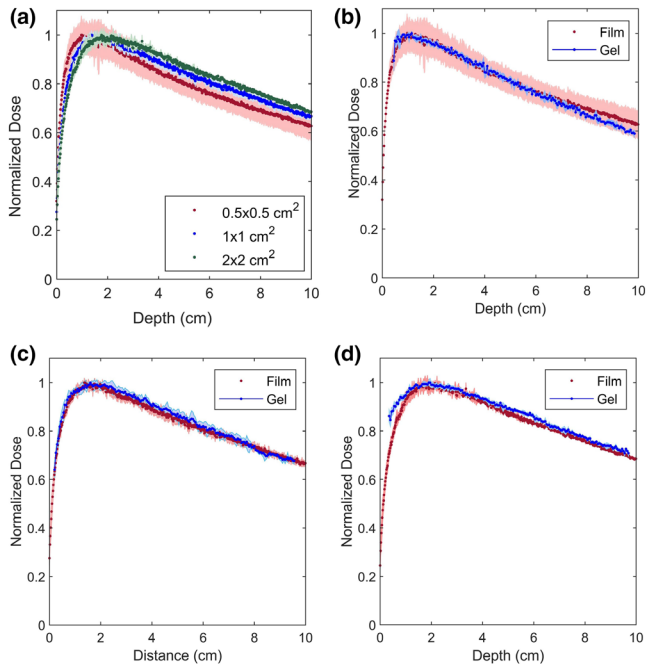


FIG. 7. PDD curves, an average of three different trials, for each of the small radiation fields (a) Film-based PDDs for all fields (b) $0.5 \times 0.5 \text{ cm}^2$, (c) $1 \times 1 \text{ cm}^2$, (d) $2 \times 2 \text{ cm}^2$ measured with gels and films. Error bars are represented for both film and gel as the point standard deviation between the three different trials. [Color figure can be viewed at wileyonlinelibrary.com]

TABLE IV. ROFs of the different Linatron field sizes relative to the $2 \times 2 \text{ cm}^2$ field.

Field Size (cm^2)	Film ROF	Gel ROF	Relative % Difference
0.5×0.5	0.70 ± 0.03	0.67 ± 0.01	4.3 %
1×1	0.89 ± 0.03	0.88 ± 0.02	1.1 %
2×2	1.00 ± 0.05	1.00 ± 0.01	0.00%

the smaller field size of $0.5 \times 0.5 \text{ cm}^2$, which could be as high as 4.18%. This uncertainty was calculated ignoring the other relevant uncertainties such as film uncertainties and the Linatron output variability as each is considered to be less than 1%. To increase the reproducibility of the lead brick positioning, we recommend for future work that the output is measured after collimation positioning prior to any experiments to maintain a higher accuracy of the dose delivery and monitoring as applied in the $2 \times 2 \text{ cm}^2$ output check for animal irradiation experiments. However, it is noticeable that with repeatability of the measurements, the overall positioning becomes more reproducible. This reproducibility is reflected with the relatively smaller relative percent difference between the gel and film measurements of the ROF that were performed on different days and with independent manual collimation setups.

The smaller collimated field ($0.5 \times 0.5 \text{ cm}^2$) exhibits higher uncertainty in the collimation placement and, therefore, higher measured collimator positioning uncertainty in

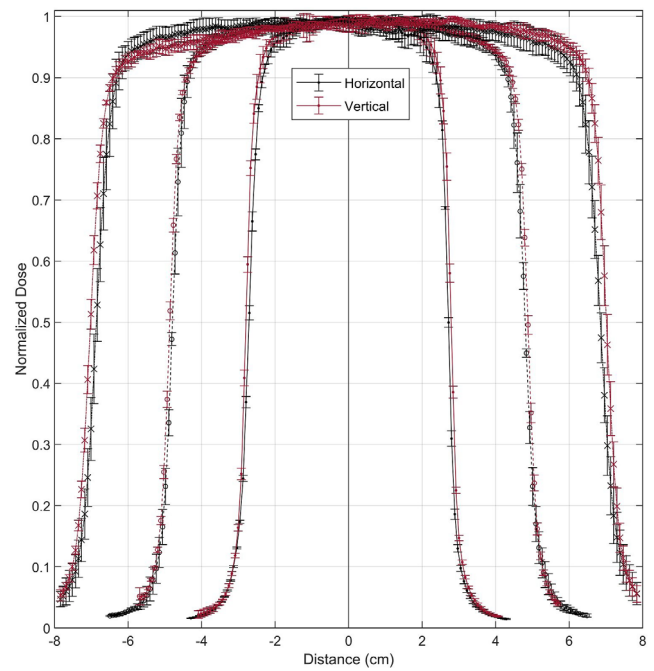


FIG. 8. Beam profiles of primary collimated Linatron beam divergence (5.08 cm diameter) with distance from the beam exit measured with films at beam exit, 1.25 m and at 2.5 m from beam exit. [Color figure can be viewed at wileyonlinelibrary.com]

TABLE V. The field size diversion data with distance from the target source

SSD (cm)	Measured Field (cm)	Calculated Field(cm)	Relative % Error
161	5.75	5.49	4.53
286	9.81	9.63	1.83
411	14.00	13.84	1.14

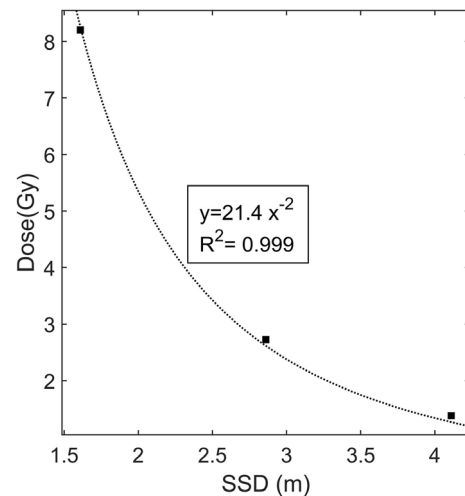


FIG. 9. Inverse-square law fitting verification of dose (in Gy) measured with films as a function of distance from source (in meters).

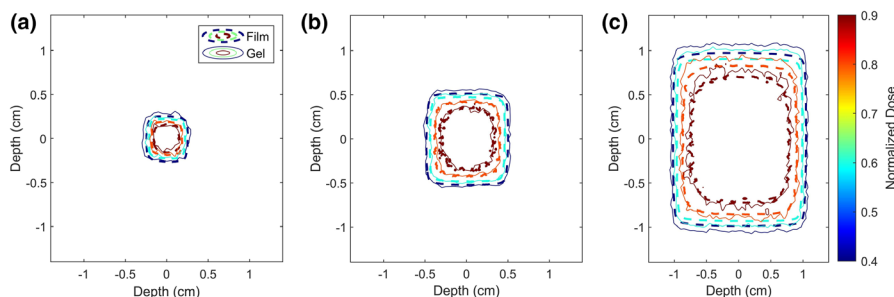


FIG. 10. Isodose contour plots of the different small-field profiles at a depth of 2 cm for gels and films. Isodose lines are 90, 80, 60, and 40%. (a) 0.5×0.5 cm² field, (b) 1×1 cm² field and (c) 2×2 cm² field. [Color figure can be viewed at wileyonlinelibrary.com]

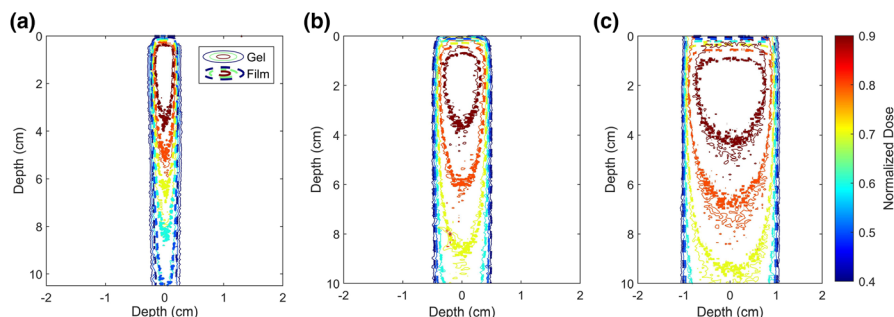


FIG. 11. Isodose contour plots (90, 80, 70, 60, 50 and 40%) for the different small-field plane PDDs for gels and films normalized to the maximum dose. (a) 0.5×0.5 cm² field, (b) 1×1 cm² field and (c) 2×2 cm² field. [Color figure can be viewed at wileyonlinelibrary.com]

comparison to the 2×2 cm² field. On the other hand, the variability of the per-field output could be 1.1 % for the case of the 1×1 cm² field when the collimation was kept in position. These measurements show that the major expected source of measurement variability is due to the positioning uncertainty of the secondary collimators. The differences in the measured beam sizes by gels to those measured with films (Table III) are a maximum of approximately 0.8 mm. The difference in the resolution of the two methods is the main cause of this discrepancy between the beam profile results. The measured ROFs for the 1×1 cm² and 0.5×0.5 cm² are within a maximum relative error of 0.8%, 12.6% from the MC simulated results. The higher error for the smaller field was mainly caused by the collimation positioning error, which was measured to be 4.18%. A 1 mm spatial displacement of the collimation position of the 0.5×0.5 field was simulated to cause a corresponding drop in the simulated ROF value by as high as 21%. Thus, that caused the measured ROF to be lower than the simulated value. In addition, Monte Carlo methods for very small fields are difficult due a range of factors, including the approximation of a point source which is unable to properly replicate potential source occlusion in dose measurements. Since our two measurement methods congruently indicate output factors lower than simulated, we believe the source occlusion could be an additional source of uncertainty.

Additionally, Fig. 6 shows limited out-of-beam dose measurement (profile edges) with Clearview gels in comparison to films due to the limited sensitivity of the gels for low doses; hence, gel profiles were limited to absolute doses above 8 Gy. This measurement was designed to exclude the

effect of background measured OD differences and exclude stray light noise. The higher error bars between various measurement trials in the profile edges (penumbra region) were due to the effect of the coarser resolution of the gels in comparison to the films as shown in Fig. 6.

The gel measured PDDs show higher uncertainty in the buildup region up to 0.5 cm due to the effect of image reconstruction artifacts from stray light and light refraction at the surface of the gel. This uncertainty limits the use of gels for surface dose measurements.^{17,47} The depth of the maximum dose, as well as the surface dose (as measured with films), increases with the field size due to the scattering within the phantom as shown in Fig. 7(a). The error between the three different trials of the film measurement is higher for the smaller field sizes due to the alignment difficulty of films at the central region of the smaller fields. Although films can provide highly accurate relative profile dose distributions, they are difficult to place parallel to the beam direction due to the higher possibility of angular misalignment with depth. Gel dosimetry was more robust and efficient in capturing the 3D dose distributions. For gel-based percent depth dose measurements, dose readings were acquired along the central ROI by averaging 2×2 mm² on each slice centered in the dose center of the field. This approach was performed to correct for any angular misalignments of gel with depth. Hence, the Clearview gel PDD at deeper depths (>3 cm) is expected to be more accurate than film acquired PDDs especially for the smaller fields of 0.5×0.5 cm² and 1×1 cm².

The depth of maximum dose was measured to be in a good agreement with the film results with a maximum of 1 mm difference. This difference is due to the uncertainty

associated with the dosimeter surface artifacts that affected the accuracy of the determination of the startup slice. This uncertainty was corrected through maximum dose alignment for the PDDs to predict well the surface slice of the Clearview gel. This uncertainty could have been eliminated by marking the relative positioning of the reference depth at the edge of the gel dosimeter. The percent difference error between film and gel acquired PDDs was <2% for depths from 0.5 cm to 8 cm. The accurate dosimetry within this depth for the $2 \times 2 \text{ cm}^2$ field is sufficient for small animal irradiations of interest.

Overall, the standard deviation between the different gel trials is much lower than the corresponding standard deviation between the film trials for measuring PDDs and ROFs. This reflects the higher intra-stability of the gel jars and hence their effectiveness for measurement reproducibility allowing multi-trials of small-field characterization with the same gel jars. Gels, therefore, allow higher measurement accuracy and reproducibility.

The 2D isodose lines show good agreement between EBT3 and the Clearview gels at a typical therapy depth of 2 cm. The isodose lines agree within 0.5 mm for the smaller fields and within 1 mm for the larger field of $2 \times 2 \text{ cm}^2$. This agreement was comparable to the reported values in literature comparing films to PRESAGE gel.¹⁷

All of the 2D PDD isodose line curves agree within approximately 2% of the maximum in the typical therapy region (1–4 cm) for the field sizes of $1 \times 1 \text{ cm}^2$ and $2 \times 2 \text{ cm}^2$. Film misalignment causes the curve to fall off more steeply for films in comparison to gel. This effect in addition to the collimation placement error of 4.18% has higher effect on the smaller field of the $0.5 \times 0.5 \text{ cm}^2$. A correction factor that relates the PDD measurement to the output dose measured across the beam direction at 2 cm depth improved the agreement between the film and gel measured PDD curves to be within ~5% in the typical therapy region (1–4 cm). Overall, the gel measured PDD curves are expected to be more accurate than those measured with film especially at deeper depths (>3 cm) as the gels have measured the full 3D data allowing for any dosimeter misalignment correction.

As a preliminary step for animal irradiations based on the full commissioning work, a verification measurement is recommended to check the $2 \times 2 \text{ cm}^2$ field output value for the field pre-animal irradiation. This will allow for more accurate dose control by minimizing the secondary collimation positioning error.

5. CONCLUSIONS

This work provides a simple and accurate commissioning process to measure the beam characteristics of an MV research accelerator with detailed 3D and 2D dosimetric evaluation for its implementation as a megavoltage irradiator for radiobiological and dosimetric studies in small animals. The effectiveness of radiochromic gel dosimetry as a robust and efficient 3D dosimetry tool for

small-field studies is verified through the relatively acceptable agreement to film measurements. The relative dosimetry results including beam profiles, PDDs and ROFs of are in good agreement with film results for all three tested small fields. These results emphasize the effectiveness of ClearView gels as a relative dosimetry tool especially given their dose rate and energy-independent response. Although, the dosimetric response of the Clearview gels is limited in the buildup region due to artifacts near the surface, 3D gel dosimeters showed the advantage of minimizing the dosimeter misalignment uncertainties, which is the main challenge in small-field measurements. Clearview Gels provided the full 3D dose measurement allowing for full representation of dose and dosimeter misalignment corrections. Although gels have limited accuracy in the surface and near surface regions, the high agreement between the different gel trials using the same gel dosimeter showed low inter-dosimeter variability. Hence, Clearview gels have the advantage of measuring multiple small fields and field parameters using the same single dosimeter.

ACKNOWLEDGMENTS

This research was supported in part by the National Institutes of Health (Grant R37CA222215). This work, and the linear accelerator loan, have been supported in part by the US Department of Homeland Security, Countering Weapons of Mass Destruction Office, Academic Research Initiative under Grant No. 2016-DN-077-ARI106. It was partially funded by Hadramout Establishment for Human Development (HEHD) fellowship and University of Michigan MCubed research funding. Clearview gels were provided by Modus Medical, London, Ontario. The authors would like to thank Cliff Hamner from the University of Wisconsin Medical Radiation Research Center for providing independent TLD dose verification.

CONFLICT OF INTEREST

The authors have no conflicts to disclose.

^{a)} Author to whom correspondence should be addressed. Electronic mail: nooraba@umich.edu

REFERENCES

1. Verhaegen F, Granton P, Tryggestad E. Small animal radiotherapy research platforms. *Phys Med Biol*. 2011;56:R55–R83.
2. Yoshizumi T, Brady SL, Robbins ME, Bourland JD. Specific issues in small animal dosimetry and irradiator calibration. *Int J Radiat Biol*. 2011;87:1001–1010.
3. Chao TC, Chen AM, Tu SJ, Tung CJ, Hong JH, Lee CC. The evaluation of 6 and 18 MeV electron beams for small animal irradiation. *Phys Med Biol*. 2009;54:5847–5860.
4. Sharma S, Narayanasamy G, Przybyla B, et al. Advanced small animal conformal radiation therapy device. *Technol Cancer Res Treat*. 2017;16:45–56.

5. Ghita M, Brown KH, Kelada OJ, Graves EE, Butterworth KT. Integrating small animal irradiators with functional imaging for advanced pre-clinical radiotherapy research. *Cancers*. 2019;11:170.
6. Crosbie JC, Anderson RL, Rothkamm K, et al. Tumor cell response to synchrotron microbeam radiation therapy differs markedly from cells in normal tissues. *Int J Radiat Oncol Biol Phys*. 2010;77:886–894.
7. Wong J, Armour E, Kazanzides P, et al. High-resolution, small animal radiation research platform with x-ray tomographic guidance capabilities. *Int J Radiat Oncol Biol Phys*. 2008;71:1591–1599.
8. Cho N, Tsiamas P, Velardeet E, et al. Validation of GPU-accelerated superposition-convolution dose computations for the Small Animal Radiation Research Platform. *Med Phys*. 2018;45:2252–2265.
9. Schreiner LJ, Olding T. “Gel Dosimetry”, in #34 Clinical Dosimetry Measurements in Radiotherapy (2009 AAPM Summer School), 2009, p. 1112.
10. “Technical Reports SeriEs No. 483: Dosimetry of Small Static Fields Used in External Beam Radiotherapy; An International Code of Practice for Reference and Relative Dose Determination”. 2017.
11. Almond PR, Biggs PJ, Coursey BM, et al. AAPM’s TG-51 protocol for clinical reference dosimetry of high-energy photon and electron beams. *Med Phys*. 1999;26:1847–1870.
12. Palmans H, Andreo P, Huq MS, Seuntjens J, Christaki KE, Meghzifene A. Dosimetry of small static fields used in external photon beam radiotherapy: summary of TRS-483, the IAEA–AAPM international Code of Practice for reference and relative dose determination. *Med Phys*. 2018;45:e1123–e1145.
13. Verhaegen F, Dubois L, Gianolini S, et al. ESTRO ACROP: technology for precision small animal radiotherapy research: Optimal use and challenges. *Radiother Oncol*. 2018;126:471–478.
14. Ma C-M, Coffey CW, DeWerd LA, et al. TG61: AAPM protocol for 40–300 kV x-ray beam dosimetry in radiotherapy and radiobiology. *Med Phys*. 2001;28:868–893.
15. “International Commission in Radiation Units and Measurements: Determination of absorbed dose in a patient irradiated by beams of X or gamma rays in radiotherapy procedures ICRU Report No. 24”, (ICRU Publications, Washington, DC), 1976.
16. Lindsay PE, Granton PV, Gasparini A, et al. Multi-institutional Dosimetric and geometric commissioning of image-guided small animal irradiators. *Med Phys*. 2014;41:1–12.
17. Newton J, Oldham M, Thomas A, et al. Commissioning a small-field biological irradiator using point, 2D, and 3D dosimetry techniques. *Med Phys*. 2011;38:6754–6762.
18. Tryggestad E, Armour M, Iordachita I, Verhaegen F, Wong JW. A comprehensive system for dosimetric commissioning and Monte Carlo validation for the small animal radiation research platform. *Phys Med Biol*. 2009;54:5341–5357.
19. Feddersen TV, Rowshanfarzad P, Abel TN, Ebert MA. Commissioning and performance characteristics of a pre-clinical image-guided radiotherapy system. *Australas Phys Eng Sci Med*. 2019;42:541–551.
20. Stojadinovic S, Low DA, Hope AJ, et al. MicroRT – Small animal conformal irradiator. *Med Phys*. 2007;34:4706–4716.
21. Pidikiti R, Stojadinovic S, Speiser M, et al. Dosimetric characterization of an image-guided stereotactic small animal irradiator. *Phys Med Biol*. 2011;56:2585–2599.
22. Zhou H, et al. “NIH Public Access”. 2011;78:297–305.
23. Clarkson R, Lindsay PE, Ansell S, et al. Characterization of image quality and image-guidance performance of a preclinical microirradiator. *Med Phys*. 2011;38:845–856.
24. Wang Y-F, Lin S-C, Na YH, Black PJ, Wu C-S. Dosimetric verification and commissioning for a small animal image-guided irradiator. *Phys Med Biol*. 2018;63:145001.
25. Silvestre Patallo I, Subiel A, Westhorpe A, et al. Development and implementation of an end-to-end test for absolute dose verification of small animal preclinical irradiation research platforms. *Int J Radiat Oncol Biol Phys*. 2020;107:587–596.
26. Haraldsson P, Bäck SÅJ, Magnusson P, Olsson LE. Dose response characteristics and basic dose distribution data for a polymerization-based dosimeter gel evaluated using MR. *Br J Radiol*. 2000;73:58–65.
27. Andrews HL, Murphy RE, LeBrun EJ. Gel dosimeter for depth-dose measurements. *Rev Sci Instrum*. 1957;28:329–332.
28. Baldock C, De Deene Y, Oldham M, Mcjury M, Pappas E, Maris T. “Physics in Medicine & Biology Related content Magnetic resonance imaging of radiation dose distributions using a polymer-gel dosimeter”. 1994.
29. Ibbott GS. Clinical applications of gel dosimeters. *J Phys Conf Ser*. 2006;56:108–131.
30. Oldham M, Siewerdsen JH, Shetty A, Jaffray DA. High resolution gel-dosimetry by optical-CT and MR scanning. *Med Phys*. 2001;28:1436–1445.
31. Aljarrah K, Sharp GC, Neicu T, Jiang SB. Determination of the initial beam parameters in Monte Carlo linac simulation. *Med Phys*. 2006;33:850–858.
32. Baldock C, De Deene Y, Doran S, et al. Polymer gel dosimetry. *Phys Med Biol*. 2010;55:R1–R63.
33. Schreiner LJ. True 3D chemical dosimetry (gels, plastics): development and clinical role. *J Phys Conf Ser*. 2015;573:12003.
34. Oldham M. Radiochromic 3D Detectors. *J Phys Conf Ser*. 2015;573:12006.
35. Gore JC, Kang YS. Measurement of radiation dose distributions by nuclear magnetic resonance (NMR) imaging. *Phys Med Biol*. 1984;29:1189–1197.
36. Maryanski MJ, Zastavker YZ, Gore JC. Radiation dose distributions in three dimensions from tomographic optical density scanning of polymer gels: II. Optical properties of the BANG polymer gel. *Phys Med Biol*. 1996;41:2705–2717.
37. Jirasek A. Considerations for x-ray CT polymer gel dosimetry. *J Phys Conf Ser*. 2013;444:12005.
38. Salomons GJ, Park YS, Kim B. Physics in Medicine & Biology Related content Polymer gel dosimetry using x-ray computed tomography: a feasibility study 4 Polymer gel dosimetry using x-ray computed tomography: a feasibility study *. 2000.
39. Vandecasteele J, De Deene Y. Evaluation of radiochromic gel dosimetry and polymer gel dosimetry in a clinical dose verification. *Phys Med Biol*. 2013;58:6241–6262.
40. Bayreder C, Georg D, Moser E, Berg A. Basic investigations on the performance of a normoxic polymer gel with tetrakis-hydroxy-methyl-phosphonium chloride as an oxygen scavenger: Reproducibility, accuracy, stability, and dose rate dependence. *Med Phys*. 2006;33:2506–2518.
41. De Deene Y, Vergote K, Claeys C, De Wagter C. The fundamental radiation properties of normoxic polymer gel dosimeters: a comparison between a methacrylic acid based gel and acrylamide based gels. *Phys Med Biol*. 2006;51:653–673.
42. Karlsson A, Gustavsson H, Månsson S, McAuley KB, Bäck SÅJ. Dose integration characteristics in normoxic polymer gel dosimetry investigated using sequential beam irradiation. *Phys Med Biol*. 2007;52:4697–4706.
43. Baldock C, De Deene Y, Doran S, et al. Polymer gel dosimetry. *Phys Med Biol*. 2010;55:1–87.
44. Guo PY, Adamovics JA, Oldham M. Characterization of a new radiochromic three-dimensional dosimeter. *Med Phys*. 2006;33:1338–1345.
45. Clear View 3D Dosimeter. [Online]. Available: <https://modusqa.com/dosimetry/dosimeters/clearview>. [Accessed: 21-Jan-2020].
46. Huet C, Colnot J, Clairand I. Preliminary investigation of the dosimetric properties of ClearView™ dosimeter. *J Phys Conf Ser*. 2017;847:2017.
47. Colnot J, Huet C, Gschwind R, Clairand I. Characterisation of two new radiochromic gel dosimeters TruView™ and ClearView™ in combination with the vista™ optical CT scanner: a feasibility study. *Phys Medica*. 2018;52:154–164.
48. Ashland Inc. “GAFChromic™ EBT3 film specifications”, 2014. [Online]. Available: http://www.gafchromic.com/documents/EBT3_Specifications.pdf. [Accessed: 21-Jan-2020].
49. V. M. Systems. “Linatron-M9 & M9A Modular high-energy X-ray source”. 7–10.
50. “EXRADIN ion chambers: Thimble ionization chambers”. 2010. [Online]. Available: http://www.teambest.com/CNMC_docs/radPhysics/thimble/CNMC_PTW_pinpoint.pdf Accessed: 21-Jan-2020.
51. Walters B, Kawrakow I, Rogers DWO. “DOSXYZnrcUsers Manual. Nrc Report Pirs”. 2005.
52. Rogers DWO, Walters B, Kawrakow I. “BEAMnrcUsers Manual. Nrc Report Pirs”. 2009.
53. Clift C, Thomas A, Adamovics J, Chang Z, Das I, Oldham M. Toward acquiring comprehensive radiosurgery field commissioning data using

- the PRESAGE®/ optical-CT 3D dosimetry system. *Phys Med Biol.* 2010;55:1279–1293.
54. Fareed A, Vavere AL, Zimmermann E, et al. Impact of iterative reconstruction vs. filtered back projection on image quality in 320-slice CT coronary angiography. *Med (United States).* 2017;96:1–5.
 55. Olding T, Schreiner LJ. Cone-beam optical computed tomography for gel dosimetry II: Imaging protocols. *Phys Med Biol.* 2011;56:1259–1279.
 56. Niroomand-Rad A, Blackwell CR, Coursey BM, et al. Radiochromic film dosimetry: recommendations of AAPM Radiation Therapy Committee Task Group 55. *Med Phys.* 1998;25:2093–2115.
 57. Ashland Inc. “User Manual FilmQA TM Pro”. 2013.
 58. Nath R, Biggs PJ, Bova FJ, et al. AAPM code of practice for radiotherapy accelerators: Report of AAPM Radiation Therapy Task Group No. 45. *Med Phys.* 1994;7:1093–1121.
 59. Butson MJ, Cheung T, Yu PKN. Absorption spectra variations of EBT radiochromic film from radiation exposure. *Phys Med Biol.* 2005;50: N135–N140.
 60. Gibbons JP, Antolak JA, Followill DS, et al. Monitor unit calculations for external photon and electron beams: Report of the AAPM Therapy Physics Committee Task Group No. 71. *Med Phys.* 2014;41:31501.
 61. Zhang W, Oraiqat I, Lei H, Carson PL, Naqa IEL, Wang X. Dual-modality X-Ray-induced radiation acoustic and ultrasound imaging for real-time monitoring of radiotherapy. *BME Front.* 2020;2020:1–10.